Proceedings of the ASME 2015 Dynamic Systems and Control Conference
DSCC2015
October 28-30, 2015, Columbus, Ohio, USA

DSCC2015-9932

EFFICIENT SPATIAL DYNAMICS FOR CONTINUUM ARMS

Isuru S. Godage*
Dept. of Mechanical Engineering
Vanderbilt University, Nashville, TN 37212
Email: isuru.godage@vanderbilt.edu

Raul Wirz
Dept. of Mechanical Engineering
Vanderbilt University, Nashville, TN 37212
Email: raul.wirz@vanderbilt.edu

Ian D. Walker
Dept. of Electrical and Computer Engineering
Clemson University, Clemson, SC 29634
Email: iwalker@g.clemson.edu

Robert J. Webster III
Dept. of Mechanical Engineering
Vanderbilt University, Nashville, TN 37212
Email: robert.webster@vanderbilt.edu

ABSTRACT

Continuum robot dynamic models have previously involved a choice between high accuracy, numerically intensive models, and low accuracy, computationally efficient models. The objective of this paper is to provide an accurate dynamic model with low computational overhead. Our approach is to place point masses at the center of gravity of the continuum section, rather than along the robot's backbone or centerline. This enables the model to match the robot's energetic characteristics with many fewer point masses. We experimentally validate the model using a pneumatic muscle actuated continuum arm. We find that the proposed model successfully captures both the transient and steady state dynamics of the arm.

INTRODUCTION

Because of their tentacle-like dexterity and inherent compliance, continuum robots are well suited for tasks in cluttered, delicate, or unstructured environments. Inspired by muscular structures such as tongues [1], elephant trunks [2, 3] and octopus arms [4,5], continuum arms can elongate, contract, and bend at any point [6, 7]. In addition to compliance and dexterity, potential advantages over traditional rigid-link robots include reduced manipulator weight, better fault tolerance [8], and human friendly interaction [9]. Based on these potential advantages, continuum robots have been increasing in popularity in recent years. However, the lack of accurate and computationally efficient dynamic models continues to prevent wider adoption of these robots, particularly in industrial settings where rapid motions are required.

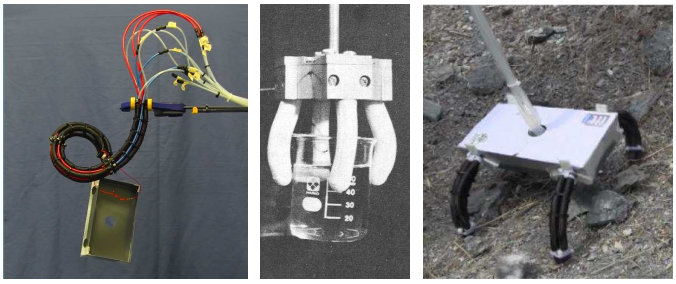

(a) (b) (c)

FIGURE 1: (a) Serial multisection continuum arm handling an object, (b) continuum sections as gentle fingers of a grasping manipulator (from [10]), (b) continuum sections as compliant limbs of a quadruped robot (from [11])

Continuum robots are made up of multiple sections, each of which can typically have its own curvature and bending plane

*Address all correspondence to this author.

[12]. Each section can be thought of as a parallel manipulator with multiple variable length (and bendable) actuators. Due to various design choices, many (though not all) continuum sections bend into circular arcs [13,14]. In this paper we will consider one such design - a pneumatically actuated robot that has been previously modeled both kinematically and dynamically in [15]. It uses Pneumatic Muscle Actuators (PMA) which are well-suited to use in continuum arms due to their high flexibility and power to weight ratio [16].

Serial multisection continuum arm prototypes (figure 1a) have been used for adaptive whole arm grasping [17], obstacle avoidance [18], navigation/inspection in obstructive environments [19,20]. Figure 1 shows some parallel multisection continuum robots. These can be used as grasping manipulators where each continuum section acts as a gentle finger (figure 1b shows handling of a glass beaker) and coordinated as limbs for locomotion (figure 1c). While the design of continuum robots has advanced rapidly in recent years, deriving dynamic models that are both accurate and efficient remains a formidable challenge. This is due to the complexity of both kinematic and mechanics models for these highly nonlinear devices.

However, a number of useful approaches have been previously reported in the literature. Parametric models represent the continuous smooth bending of continuum arms [21] but the tradeoff is that they map the modeled robots configurations to a restricted set of motion "shapes". Theoretical modeling for an inextensible, unidimensional cable robot was reported in [22] but typical continuum arms have multiple degrees of freedom. Elliptic integrals were used in [23] to model continuum sections but it only accounted for statics of the robot without considering the gravitational potential energy. Therefore the model cannot be applied for dynamic simulations of macro-scale continuum arms where gravity effect is significant. Cosserat rod theory was used to model inextensible tendon actuated continuum sections in [24–26] but the authors did not attempt to address the computationally efficiency of the resulting model. The modal kinematics for continuum arms [27] combined the structural accuracy of curve parametric models and numerical efficiency/stability of modal methods. Utilizing the modal kinematics, spatial dynamics for continuum sections were proposed in [8, 15]. However, these models were based on integral formulations and therefore computationally intensive and not suitable for rapid simulations.

Composed of a small number of rigid-linked segments or mass points along the length, lumped parameter models of continuum arms avoid complex integral expressions and produce efficient results. However, to approximate the smooth bending of continuum arms, many segments or mass points are required [28]. This significantly increases the overall degrees of freedom in contrast to actual number of controlled joint variables along with the computational complexity. The lumped model in [29] used curve parametric models for the derivation but has numerical instabilities for straight arm poses [8]. The model proposed in [30] only used 3 segments but does not represent the mass distribution of continuum sections. Further, all the lumped models so far focus solely on reducing computational complexity without analyzing the accuracy of the model in comparison to actual system in the energy domain.

Employing the modal kinematics proposed in [12, 27], this paper presents a single mass, lumped parameter spatial dynamic model for continuum arms. Unlike previously reported lumped models, this approach investigates the mass-related energy of continuum arms to derive the best representation of the entire system using only a single lumped mass. The result is a model that is both simple and computationally efficient. Lastly, we experimentally validate the model using a prototype PMA actuated continuum arm. Note that while this paper was in the review process, the results described herein were extended to archival form and published in [31].

PROTOTYPE CONTINUUM ARM

The prototype continuum section shown in figure 2a consists of three mechanically identical extending PMA's [32] with unactuated length $L_0 = 0.22m$, lower and upper bounds of the length variation $l_{min} = 0m$, and $l_{max} = 0.071m$ within the operation pressure range $(0-5bars)$. Due to the gradual pressure buildup in PMA's, the maximum joint-space velocity is $0.16ms^{-1}$. Silicone tubes of inner diameter (ID) $10mm$ and outer diameter (OD) $13mm$ make the PMA bladders. Nylon union tube connectors $(ID = 6mm)$ seal the Silicone tubes at either end. The pressure-supplying Polyethylene tubes connected to union connectors provide the pressure inputs. The Polyester braided sheath $(OD = 13-26mm)$ is then inserted and tightened with high strength Nylon cable ties. Rigid plastic mount frames of $r = 0.016m$ and $2.54mm$ thickness (see figure 2b, top right) are used to mount the PMAs. Rigid circular plastic constrainers (figure 2b, bottom right) help constrain PMA's to operate parallel to the neutral axis at designated clearance $\left(\frac{2\pi}{3}rad \text{ apart at } r\right)$ from each other as well as provide improved torsional stiffness. The complete continuum arm has a mass (m) of $0.168kg$. The pressure to each PMA is controlled by a Pneumax® 171E2N.T.D.0009S digital proportional pressure regulator which is controlled through a RS232 digital command-response type interface that support real-time pressure commanding and reading. NDI Aurora tabletop magnetic tracking system provided the tip position at 30 times per second at a mean accuracy of $0.008m$.

Figure 3a shows the schematic of the prototype continuum arm shown in figure 2a. Variable length continuum arms generate motion by elastic deformation and this causes the length of the neutral axis to vary, hence the term variable length. As a result, the points along the arm have varying relative position and orientations. The length of an actuator at any time is $L_j = L_0 + l_j(t)$ where $0 \leq l_j(t) \leq l_{max}$, $j \in \{1,2,3\}$ and t is the time.

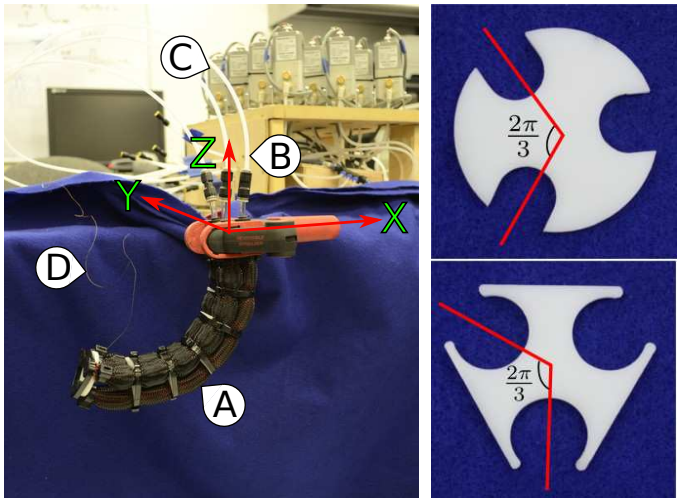

(a) (b)

FIGURE 2: (a) The pneumatic muscle actuated variable length continuum section: A:-continuum section, B:-pressure supplying tubes, C:-Pneumax 171E2N.T.D.0009S digital pressure controllers, D:-NDI magnetic coil sensor for tip trajectory tracking, (b) rigid PMA mount frame (top right) where the grooves house union tube connectors. The constrainer plates (bottom right) and the groves support PMA's along the length.

METHODOLOGY

In this section, the continuum arm energy is studied in terms of integral Lagrangian and traditional lumped mass (along the neutral axis) approaches. The insights gained are used to derive the new lumped parameter dynamic model. The following modeling assumptions are made:

1. Continuum sections are constant curvature
2. The robot's mass within each section is constant and uniform in linear density
3. All robot cross sections are symmetric

Validity of the Assumptions

The evenly installed constrainers (support disks) along our prototype continuum arm prevent twisting about the neutral axis ensuring assumption 1. Also, many prior continuum robots exhibit constant curvature [13], and the modal kinematics derived previously for this robot [12, 27] were based on this assumption. The amount of air in each continuum section is much less than the mass of the robot, and can hence be neglected. Further, the PMA's and constrainers are uniformly distributed along the length of continuum arm thus conforms to assumption 2. Moreover, the PMA's are tightly bundled cylindrically and comply with the assumption 3.

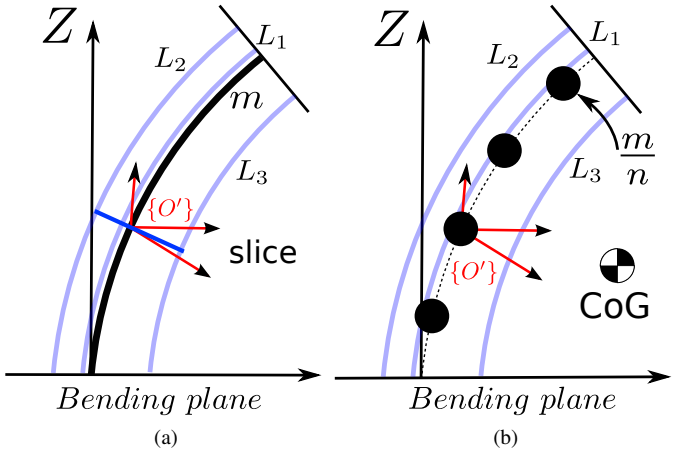

(a) (b)

FIGURE 3: (a) Schematic diagram of a continuum section with uniformly distributed mass along the length. An infinitesimally thin slice at $\{O'\}$ is also shown. (b) schematic of a lumped mass system with n number of point masses along the length. The center of gravity (CoG) is also marked.

Review of Modal Dynamics

The equations of motion for single continuum sections proposed in [15] was based on the integral Lagrangian approach. The model was theoretically accurate, accounted both linear and angular kinetic energies (KE) as well as gravitational, elastic potential energies (PE). Due to the complexity of the derivation it is difficult to extend the model to multisection applications.

Herein, the integral Lagrangian is revisited to investigate the KE and PE of the system in detail to compare with the traditional and proposed lumped models. From [12], define the modal homogeneous transformation matrix of the prototype arm, $\mathbf{T} \in SE(3)$, as

$$\mathbf{T}(\xi,q) = \begin{bmatrix} \mathbf{R}(\xi,q) & p(\xi,q) \\ \mathbf{0} & 1 \end{bmatrix}, \tag{1}$$

where $q = [l_1, l_2, l_3]^T \in \mathbb{R}^3$, $\mathbf{R} \in SO(3)$ is the rotation matrix and $p \in \mathbb{R}^3$ is the position vector of the neutral axis. The scalar $\xi \in [0,1]$ defines the moving coordinate frame along the neutral axis while $\xi = 1$ is the tip.

Let the Lagrangian of the system be $\mathscr{L} = \mathscr{K} - \mathscr{P}$ where $\mathscr{K}$ and $\mathscr{P}$ are KE and PE. Assume that the continuum arm is composed of thin slices (see figure 3a). The slice linear $(\upsilon \in \mathbb{R}^3)$ and angular $(\omega \in \mathbb{R}^3)$ velocities relative to $\{O'\}$ are

$$\upsilon(\xi,q) = \mathbf{R}^T \dot{p}, \tag{2}$$

$$\omega(\xi,q) = (\mathbf{R}^T \dot{\mathbf{R}})^{\vee}, \tag{3}$$

where $\vee$ operator extracts the velocity elements from the skew symmetric angular velocity matrix. The dependency variables are omitted from here onward for brevity.

From [8], the mass of a slice is $m\delta\xi$. Integrating the mass related slice energies with respect to ξ, the total linear KE ($\mathscr{K}^{\upsilon}$), angular KE, ($\mathscr{K}^{\omega}$), and gravitational PE ($\mathscr{P}^{g}$) are given by

$$\mathscr{K}^{\upsilon} = \frac{1}{2}\int_0^1 \left(\upsilon^T \mathscr{M}^{\upsilon} \upsilon\right) d\xi, \tag{4}$$

$$\mathscr{K}^{\omega} = \frac{1}{2}\int_0^1 \left(\omega^T \mathscr{M}^{\omega} \omega\right) d\xi, \tag{5}$$

$$\mathscr{P}^{g} = m\int_0^1 \left(p^T g\right) d\xi, \tag{6}$$

where $\mathscr{K} = \mathscr{K}^{\upsilon} + \mathscr{K}^{\omega}$, $\mathscr{M}^{\upsilon} = m\mathbf{I}_3$ contains the linear moments of inertia, $\mathscr{M}^{\omega} = \frac{mr^2}{4}\,\mathrm{Diag}(1,1,2)$ contains the angular moments of inertia (from assumption 3 of symmetry), $\mathbf{I}_3$ is the rank 3 identity matrix, and $g = [0,0,-9.81]^T$ is the gravity vector.

Energy Analysis and Model Reduction

In this section, mass related integral energy terms are investigated for possible simplifications. Employing the "global search" on "fmincon" constrained optimization technique in MATLAB with the prototype parameter values and ranges, it was computed that $\mathscr{K}^{\omega}/\mathscr{K} \leq 3\%$. Therefore, $\mathscr{K}^{\omega}$ can be safely neglected to assume $\mathscr{K} \approx \mathscr{K}^{\upsilon}$. Now the mass of the arm is considered to be distributed along the neutral axis. But from (4) and (6), it can be seen that even with these assumptions and simplifications, an integral approach is still required. Fortunately, a lumped mass model can avoid this.

Consider that the continuum arm mass is uniformly distributed at n points along the neutral axis as shown in figure 3b. Hence, each mass point, $\frac{m}{n}$ is at $\xi = \frac{j}{n} \forall j \in [1,n]$ and the total KE ($\mathscr{K}_n$) and gravitational PE ($\mathscr{P}_n^g$) of the lumped system of n points is computed as

$$\mathscr{K}_n = \frac{m}{2n}\sum_{j=1}^{n} \dot{p}^T\left(q,\frac{j}{n}\right)\dot{p}\left(q,\frac{j}{n}\right), \tag{7}$$

$$\mathscr{P}_n^g = \frac{m}{n}\sum_{j=1}^{n} p^T\left(q,\frac{j}{n}\right) g. \tag{8}$$

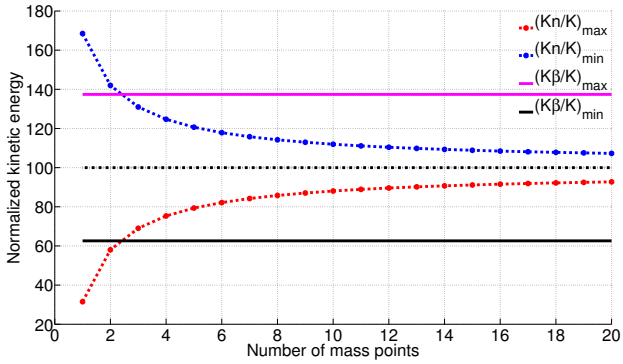

FIGURE 4: Normalized kinetic energy ranges of $\mathscr{K}_n/\mathscr{K}$ for different discrete points masses and CoG lumped mass, $\mathscr{K}_\beta/\mathscr{K}$.

Employing the "global search" on "fmincon" constrained optimization routine, percentage ranges of $\mathscr{K}_n/\mathscr{K}$ and $\mathscr{P}_n^g/\mathscr{P}^g$ were computed for increasing n. The normalized KE and gravitational PE variation are plotted in figures 4 and 5. Normalization was done so that the mean of the variation range equals the integral system energies, $\mathscr{K}^{\upsilon}$ and $\mathscr{P}^g$ (i.e., 100%). The plots clearly indicate that low fidelity (low n) lumped models have large energy variance and hence poorly capture the behavior of the physical prototype in the energy domain. But using a large n is also not desirable because it increases computational complexity.

Now, for the same continuum arm, consider that the mass is concentrated at the center of gravity (CoG), as shown in figure 3b. Note that, the CoG plays a vital role in rigid body dynamics; it is where the body coordinates are typically assigned for evaluating dynamics. This enables KE and PE computation without moment of inertia coordinate transformations. However, this approach has not been studied for deriving the dynamics of continuum arms. The CoG position vector relative to $\{O\}$, $\beta \in \mathbb{R}^3$, can be calculated as

$$\beta(q) = \frac{m\int_0^1 p(q,\xi)\,d\xi}{m} = \int_0^1 p(q,\xi)\,d\xi. \tag{9}$$

The CoG KE ($\mathscr{K}^{\beta}$) and gravitational PE ($\mathscr{P}_{\beta}^{g}$) are given by

$$\mathscr{K}^{\beta} = \frac{1}{2} m\dot{\beta}^T\dot{\beta}, \tag{10}$$

$$\mathscr{P}_{\beta}^{g} = m\beta^T g = \mathscr{P}^g. \tag{11}$$

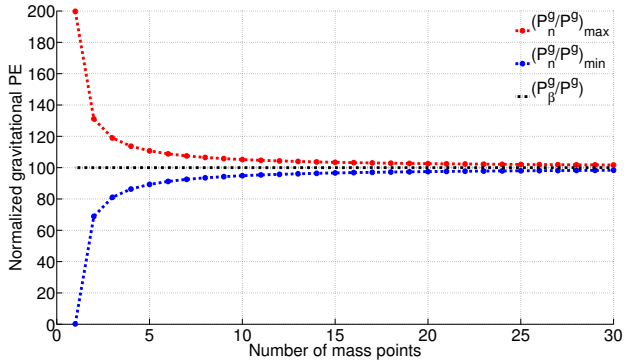

FIGURE 5: Normalized gravitational potential energy ranges of $\mathscr{P}^g_n/\mathscr{P}^g$ for different discrete points masses and CoG lumped mass, $\mathscr{P}^g_\beta/\mathscr{P}^g$.

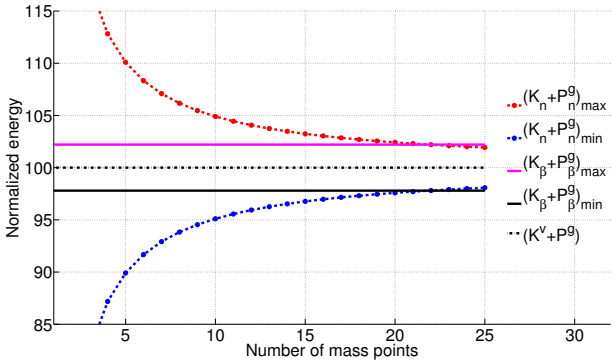

FIGURE 6: Normalized combined gravitational PE and KE ranges of $\mathscr{K}_n+\mathscr{P}^g_n/\mathscr{K}+\mathscr{P}^g$ for different discrete points masses and CoG lumped mass, $\mathscr{K}_\beta+\mathscr{P}^g_\beta/\mathscr{K}+\mathscr{P}^g$.

Employing the "global search" with "fmincon" constrained optimization technique in MATLAB using the prototype parameter values, $\mathscr{K}_\beta/\mathscr{K}$ and $\mathscr{P}^g_\beta/\mathscr{P}^g$ were calculated and the normalized range is plotted in figures 4 and 5. From the energy plots it can be seen that the CoG KE energy variation is comparable to a lumped model of $n=3$ but only using a single mass point. But the gravitational PE exactly matches the integral system model given in (6). The equations of motion of the continuum arm contains the effects of both KE and PE. Now the combined effect of KE and PE is computed. Utilizing the same "global search" optimization with "fmincon", the range of $\mathscr{K}_n+\mathscr{P}^g_n/\mathscr{K}+\mathscr{P}^g$ is computed for varying n and figure 6 shows the results. Similarly, the range of $\mathscr{K}_\beta+\mathscr{P}^g_\beta/\mathscr{K}+\mathscr{P}^g$ is also plotted in figure 6. It is evident that the proposed CoG approach is comparable to a lumped model of n=22 without the computational burden. Further, with the CoG approach, preintegration of product of integrable terms such as (4) is no longer required. Thus only β given in (9) and its partial derivatives with respect to q have to be precomputed. This results a in considerable time saving with regards to number of functions need to be implemented and evaluated during simulations or real-time robot operations.

IMPLEMENTATION OF THE DYNAMIC MODEL

Let the Lagrangian of CoG of the continuum arm be $\mathscr{L}_\beta = \mathscr{K}_\beta - \mathscr{P}_\beta$ where $\mathscr{K}_\beta$ is given by (10). Here, $\mathscr{P}_\beta = \mathscr{P}^g_\beta + \mathscr{P}^e_\beta$ where $\mathscr{P}^e_\beta = \frac{1}{2} q^T \mathbf{K}^e q$ is the elastic PE of PMAs and $\mathbf{K}^e = \text{Diag}\left\{K^e_1, K^e_2, K^e_3\right\} \in \mathbb{R}^{3\times3}$ is the elastic stiffness coefficient matrix. Also, define CoG velocity Jacobian as $\mathbf{J}^\beta = (\nabla_q \beta) \in \mathbb{R}^{3\times3}$ where $\nabla_q = [\frac{\partial}{\partial l_1}, \frac{\partial}{\partial l_2}, \frac{\partial}{\partial l_3}]$. From classical Lagrangian mechanics, the generalized inertia matrix of the dynamic system, $\mathbf{M} \in \mathbb{R}^{3\times3}$, is given by

$$\mathbf{M} = m_\beta \left(\mathbf{J}^\beta\right)^T \mathbf{J}^\beta, \tag{12}$$

where $m_\beta = \frac{m}{\sigma}$ and $\sigma = 0.57$ is the normalization scalar (i.e., mean of the $\mathscr{K}^\beta/\mathscr{K}$ range) used in figure 4. This way, the KE of the CoG system is well approximated to the actual system KE given by (4) by balancing $\mathscr{K}_\beta/\mathscr{K}$ variation.

The Coriolis/Centrifugal matrix can be computed from Christoffel symbols [8] using the partial derivatives of $\mathbf{M}$. Let $\mathbf{H}^\beta_j = \left(\frac{\partial}{\partial l_j}\mathbf{J}^\beta\right) \in \mathbb{R}^{3\times3}$. Therefore from (12), the j^{th} partial derivative of $\mathbf{M}$ is given by

$$\frac{\partial}{\partial l_j}\mathbf{M} = m_\beta \left\{ \left(\mathbf{H}^\beta_j\right)^T \mathbf{J}^\beta + \left(\mathbf{J}^\beta\right)^T \mathbf{H}^\beta_j \right\}. \tag{13}$$

The conservative force vector, $G \in \mathbb{R}^3$, is obtained by taking the partial derivatives of the PE's. Thus, let $G = G^g + G^e$ where $G^g = \nabla_q \mathscr{P}^g_\beta$ and $G^e = \nabla_q \mathscr{P}^e_\beta$ are given by

$$G^g = \nabla_q \mathscr{P}^g_\beta = m_\beta \left(\nabla^T_q \beta^T\right) g = m_\beta \left(\mathbf{J}^\beta\right)^T g, \tag{14}$$

$$G^e = \nabla_q \mathscr{P}^e_\beta = \mathbf{K}^e q. \tag{15}$$

Parameter Estimation

PMA's have finite operation range and by defining stiffness coefficients of $\mathbf{K}^e\left(K^e_j\right)$ as a function of length variation (l_j), the

mechanical limits can be emulated. This is achieved by assigning a high stiffness value, K^e_{max}, beyond maximum and minimum length variations and the actual stiffness value, K^e_{min}, otherwise as given by

$$K^e_j = K^e_{min} + \frac{1}{2} K^e_{max} (2 + \Lambda_1 - \Lambda_2), \tag{16}$$

where $j \in \{1,2,3\}$, $\Lambda_1 = \tanh\{\mu (l_j - l_{max})\}$, $\Lambda_2 = \tanh\{\mu (l_j - l_{min})\}$, and $\mu = 2000$.

In addition, PMAs exhibit high damping and to model these dissipative terms, simple damping coefficient, D, is used in this paper. Hence the equations of motion employed in simulation is given by

$$\mathbf{M}\ddot{q} + \mathbf{C}\dot{q} + \mathbf{D}\dot{q} + G = \tau_e, \tag{17}$$

where $\mathbf{D} = D\mathbf{I}_3 \in \mathbb{R}^{3\times3}$ and $\tau_e \in \mathbb{R}^3$ is the input force vector.

The elastic stiffness limiting values of (16) and damping coefficients in (17) were approximated experimentally. Each PMA of the prototype arm is provided with a step input of 2bars and the dynamic response is recorded. Then, the dynamic response of the model for the same input pressure profile is tuned to match the experimental results by varying K^e_j and the damping coefficient. The individual K^e_j and damping values are then used to calculate the mean values for the prototype arm. This yielded $K^e_{min} = 2650 Nm^{-1}$ and $K^e_{max} = 10^6 Nm^{-1}$ (rounded to the closest 50) and $D = 130$ (rounded to the closest 10). Note that, the prototype arm is highly constrained and has many friction sources. Since the contribution of this paper is with respect to dynamic model simplification, the hysteretic effects are not modeled. Interested readers are referred to [32] for details on hysteretic modeling. The numerical computations of (17) were carried out in MATLAB SIMULINK platform with variable-step ODE15s routine for its speed in handling complex dynamic systems. The simulation outputs were recorded at 30 data samples per second to match with the task-space tracking system we use in the experiments described in the following section.

DYNAMIC MODEL VALIDATION

To date, most of the experimental validations related to PMA actuated, variable length continuum arms have been restricted to static poses. Here the proposed model results are compared to dynamic response of the prototype arm (shown in figure 2a). The experiments are carried out prior to simulations and the pressure profiles relevant to the experiments are recorded. These pressure profiles are then used as the pressure inputs for dynamic simulations.

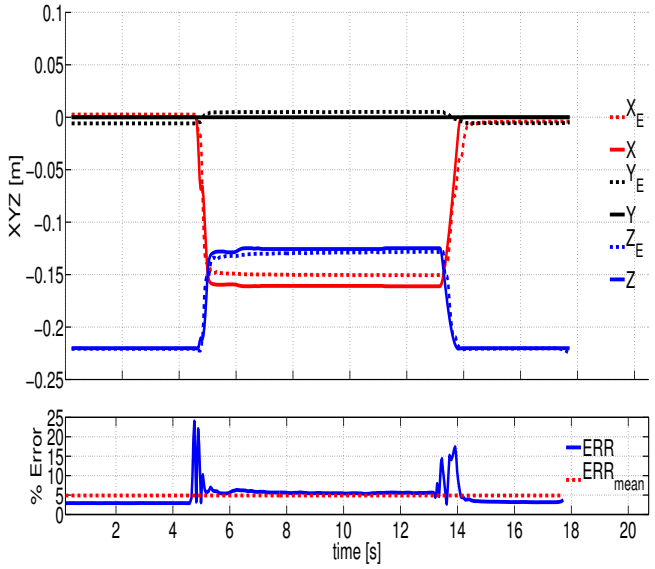

FIGURE 7: Dynamic result comparison for rectangular pulse response with normalized tip error. The dashed lines denote the experimental results while the solid lines represent the simulation results.

Rectangular Pulse Response

In this experiment, l_1 is provided a rectangular pulse input of 3bar starting at $t = 4.3s$ with duration of 8s. This causes the continuum arm to bend in a circular arc shape in the XZ plane. The experimental result comparison of the continuum arm shown in figure 2a to the dynamic model is shown in figure 7. The normalized tip error (the Euclidean distance as percentage of the continuum arm unactuated length, L_0) is also plotted for comparison. It can be seen that overall the model successfully simulates and predicts the dynamic response of the arm. It is observed that there are considerable transient errors (up to 25%) during rapid pressure changes at the rectangular input with low steady state error (4-6%) and 5% mean error during the simulation. Note that, given the high dynamic nature of the input signal, the proposed model produces good results. The discrepancies during transients can be attributed to the simple elastic stiffness and damping coefficients employed in the model without hysteretic/friction modeling. The simulation of this 17.5s experiment in MATLAB SIMULINK environment (without any optimization) took around 2s using a computer with 3.1GHz Intel i7 processor where a step of the dynamic model consumes only 305μs. This computation time can further be improved by using a compiled programming language.

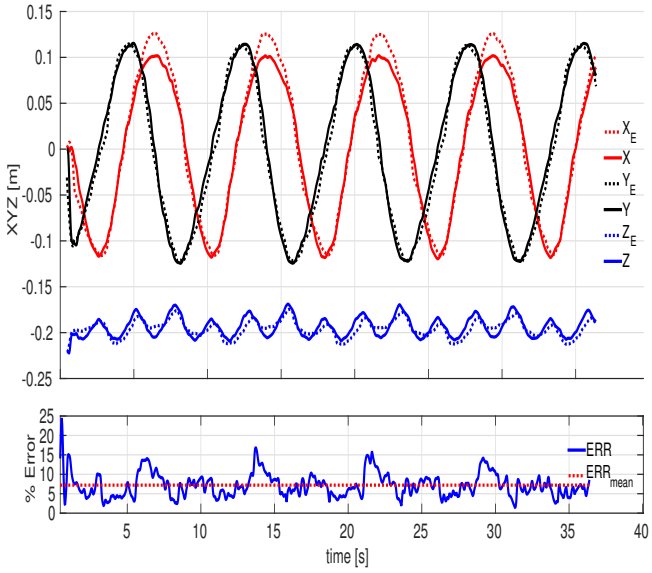

FIGURE 8: Dynamic result comparison for phase shifted sinusoidal response with normalized tip error. The dashed lines denote the experimental results while the solid lines represent the simulation results.

Phase Shifted Sinusoidal Response

In contrast to the previous experiment, this experiment uses a complex, time varying, pressure input involving all three PMAs. The input signal for any j^{th} PMA is described by $3+3\sin(\omega t+2\pi(j-1)/3)$bars where $\omega=0.9$, which is a sinusoidal pressure input phase shifted by 120°. This causes the prototype arm to move in a near circular task-space trajectory. Figure 8 compares the simulation and experimental trajectories. From the figure it is seen that there is a good agreement overall. Both Y and Z coordinate results match well while some errors are observed at X coordinate which cause the 17% error peaks of the normalized error plot. This could be a currently unmodeled, complex hysteretic phenomena when all the PMAs are actuated simultaneously. The mean error throughout the experiment is 7% which is excellent given the simplicity of the model. Further, only 6s of computational time was used for producing the simulation result of this 37s experiment in MATLAB SIMULINK environment (without any optimization). Thus, the model is suitable for real-time simulation computation and control implementations.

CONCLUSIONS

Dynamic modeling of variable length continuum arms has previously involved computationally intensive integral Lagrangian approaches. Lumped models eliminate this complexity at the cost of accuracy. This paper proposes a new lumped dynamic model for continuum arms with higher accuracy. This was achieved by investigating the energy of the actual continuum arm system and then determining the lumped mass placement for best energy agreement and numerical efficiency. The CoG lumped mass produced comparable results to a lumped parameter approximation with 22 discrete masses, but without the computational overhead. Experimental validation of the model was carried out using a PMA-actuated continuum arm. Results showed that the model successfully simulates the transient and steady state dynamics of the prototype arm. Furthermore, the proposed model can be extended to any geometrically constrained variable length continuum arm of any actuator configuration and also to multisection continuum arms.

REFERENCES

[1] Takanobu, H., Tandai, T., and Miura, H., 2004. "Multi-dof flexible robot base on tongue". In IEEE Int. Conf. on Robotics and Automation, pp. 2673–2678.

[2] Hannan, M. W., and Walker, I. D., 2000. "Analysis and initial experiments for a novel elephant's trunk robot". In IEEE/RSJ Int. Conf. on Intelligent Robots and Systems, Vol. 1, pp. 330–337.

[3] Santiago, J. L. C., Walker, I. D., and Godage, I. S., 2015. "Continuum robots for space applications based on layer-jamming scales with stiffening capability". In IEEE Aerospace Conference, pp. 1–13.

[4] Renda, F., Giorelli, M., Calisti, M., Cianchetti, M., and Laschi, C., 2014. "Dynamic model of a multibending soft robot arm driven by cables". *IEEE Tran. on Robotics,* ***30***(5), pp. 1109–1122.

[5] Tonapi, M. M., Godage, I. S., Vijaykumar, A. M., and Walker, I. D., 2015. "Spatial kinematic modeling of a long and thin continuum robotic cable". In IEEE Int. Conf. on Robotics and Automation, pp. 3755–3761.

[6] Trivedi, D., Rahn, C. D., Kier, W. M., and Walker, I. D., 2008. "Soft robotics: Biological inspiration, state of the art, and future research". *Applied Bionics and Biomechanics,* ***5***(3), pp. 99–117.

[7] Kim, Y., Cheng, S. S., and Desai, J. P., 2015. "Towards the development of a spring-based continuum robot for neurosurgery". In SPIE Medical Imaging, International Society for Optics and Photonics, pp. 94151Q–94151Q.

[8] Godage, I. S., Branson, D. T., Guglielmino, E., Medrano-Cerda, G. A., and Caldwell, D. G., 2011. "Shape function-based kinematics and dynamics for variable length continuum robotic arms". In IEEE Int. Conf. on Robotics and Automation, pp. 452–457.

[9] Walker, I. D., Dawson, D. M., Flash, T., Grasso, F. W., Hanlon, R. T., Hochner, B., Kier, W. M., Pagano, C. C., Rahn, C. D., and Zhang, Q. M., 2005. "Continuum robot arms

inspired by cephalopods". In Procs. of the Int. Society for Optical Engineering, pp. 303–314.

[10] Suzumori, K., Kondo, F., and Tanaka, H., 1993. "Micro-walking robot driven by flexible microactuator". *Journal Robotics and Mechatronics,* ***5***(6), pp. 537–541.

[11] Godage, I. S., Nanayakkara, T., and Caldwell, D. G., 2012. "Locomotion with continuum limbs". In IEEE/RSJ Int. Conf. on Intelligent Robots and Systems, pp. 293–298.

[12] Godage, I. S., Medrano-Cerda, G. A., Branson, D. T., Guglielmino, E., and Caldwell, D. G., 2015. "Modal kinematics for multisection continuum arms". *Bioinspiration & biomimetics,* ***10***(3), p. 035002.

[13] Webster III, R. J., and Jones, B. A., 2010. "Design and kinematic modeling of constant curvature continuum robots: A review". *The Int. Journal of Robotics Research,* ***29***(13), pp. 1661–1683.

[14] Godage, I. S., and Walker, I. D., 2015. "Dual quaternion based modal kinematics for multisection continuum arms". In IEEE Int. Conf. on Robotics and Automation, pp. 1416–1422.

[15] Godage, I. S., Branson, D. T., Guglielmino, E., Medrano-Cerda, G. A., and Caldwell, D. G., 2011. "Dynamics for biomimetic continuum arms: A modal approach". In IEEE Int. Conf. on Robotics and Biomimetics, pp. 104–109.

[16] Caldwell, D. G., Medrano-Cerda, G. A., and Goodwin, M., 1995. "Control of pneumatic muscle actuators". *IEEE Control Systems Magazine,* ***15***(1), pp. 40–48.

[17] McMahan, W., and Walker, I. D., 2008. "Octopus-inspired grasp-synergies for continuum manipulators". In IEEE Int. Conf. on Robotics and Biomimetics, pp. 945–950.

[18] Godage, I. S., Branson, D. T., Guglielmino, E., and Caldwell, D. G., 2012. "Path planning for multisection continuum arms". In IEEE Int. Conf. on Mechatronics and Automation, pp. 1208–1213.

[19] Mehling, J. S., Diftler, M. A., Chu, M., and Valvo, M., 2006. "A minimally invasive tendril robot for in-space inspection". In IEEE/RAS-EMBS Int. Conf. on Biomedical Robotics and Biomechatronics, pp. 690–695.

[20] Tonapi, M. M., Godage, I. S., and Walker, I. D., 2014. "Next generation rope-like robot for in-space inspection". In IEEE Procs. on Aerospace Conference, pp. 1–13.

[21] Chirikjian, G. S., 1993. "A continuum approach to hyper-redundant manipulator dynamics". In IEEE/RSJ Int. Conf. on Intelligent Robots and Systems, pp. 1059–1066.

[22] Mochiyama, H., 2006. "Hyper-flexible robotic manipulators". In IEEE Int. Symp. on Micro-NanoMechatronics and Human Science, IEEE, pp. 41–46.

[23] Xu, K., and Simaan, N., 2010. "Analytic formulation for kinematics, statics, and shape restoration of multibackbone continuum robots via elliptic integrals". *Journal of Mechanisms and Robotics,* ***2***(1), p. 011006.

[24] Rucker, D. C., and Webster, R. J., 2011. "Statics and dynamics of continuum robots with general tendon routing and external loading". *IEEE Tran. on Robotics,* ***27***(6), pp. 1033–1044.

[25] Rone, W. S., and Ben-Tzvi, P., 2014. "Mechanics modeling of multisegment rod-driven continuum robots". *Journal of Mechanisms and Robotics,* ***6***(4), p. 041006.

[26] Xu, K., Fu, M., and Zhao, J., 2014. "An experimental kinestatic comparison between continuum manipulators with structural variations". In IEEE Int. Conf. on Robotics and Automation, pp. 3258–3264.

[27] Godage, I. S., Guglielmino, E., Branson, D. T., Medrano-Cerda, G. A., and Caldwell, D. G., 2011. "Novel modal approach for kinematics of multisection continuum arms". In IEEE/RSJ Int. Conf. on Intelligent Robots and Systems, pp. 1093–1098.

[28] Zheng, T., Branson, D. T., Kang, R., Cianchetti, M., Guglielmino, E., Follador, M., Medrano-Cerda, G. A., Godage, I. S., and Caldwell, D. G., 2012. "Dynamic continuum arm model for use with underwater robotic manipulators inspired by octopus vulgaris". In IEEE Int. Conf. on Robotics and Automation, pp. 5289–5294.

[29] Rone, W., and Ben-Tzvi, P., 2014. "Continuum robot dynamics utilizing the principle of virtual power". *IEEE Tran. on Robotics,* ***30***(1), Feb, pp. 275–287.

[30] Giri, N., and Walker, I. D., 2011. "Three module lumped element model of a continuum arm section". In IEEE/RSJ Int. Conf. on Intelligent Robots and Systems, pp. 4060–4065.

[31] Godage, I. S., Wirz, R., Walker, I. D., and Webster III, R. J., 2015. "Accurate and efficient dynamics for variable length continuum arms: A center of gravity approach (in press)". *Soft Robotics*.

[32] Godage, I. S., Branson, D. T., Guglielmino, E., and Caldwell, D. G., 2012. "Pneumatic muscle actuated continuum arms: Modelling and experimental assessment". In IEEE Int. Conf. on Robotics and Automation, pp. 4980–4985.